Determining Abrasion Resistance of Decorative Coated Wood-Based Panels Using Retinex Model

Serdar Kaçamer,[a,*] Ferzan Katırcıoğlu,[b] and Mehmet Budakçı [c]

An Image Processing Based Scrub Tester (IPBST) was used to imitate the effect of household chemicals on furniture and decoration elements. For this purpose, 8 mm-thick, bright white, acrylic coated medium density fiberboard (MDF), polyvinyl chloride coated MDF, MDF lam ready-to-use sheets, and cellulosic, polyurethane, acrylic, and water-based paint applied MDF sheets were used. Carbon fiber patterned decorative coating was applied to the prepared sample surfaces using the water transfer printing and ultraviolet printing methods. The surfaces of the samples were scrubbed with various household chemicals in accordance with the Turkish Standard TS EN ISO 11998. In the image processing phase, the images before and after scrubbing were first converted to hue, saturation, and value color space. The relationship between the abrasion measurement method of the proposed IPBST and the abrasion data obtained from the stereo microscope device was examined using the Pearson Correlation analysis. The relationship between both abrasion test methods was positive, very strong, and significant (0.81). Thus, the IPBST can be used as an alternative to industrial test devices as it obtains similar data.

DOI: 10.15376/biores.19.1.1058-1078

Keywords: Wood-based medium density fiberboard (MDF) panels; Image processing; Coating; Scrub tester; Abrasion measurement

Contact information: a: Department of Design, Bolu Vocational School of Technical Sciences, Bolu Abant İzzet Baysal University; 14030, Bolu, Türkiye; b: Department of Mechatronics Engineering, Faculty of Engineering, Düzce University; 81060, Düzce, Türkiye; c: Department of Wood Products Industrial Engineering, Faculty of Forestry, Düzce University; 81060, Düzce, Türkiye;
** Corresponding author: serdar.kacamer@ibu.edu.tr*

INTRODUCTION

Protective layers such as paint, varnish, and coating are used to increase the aesthetic value of wood-based composite panels and to ensure their resistance against external factors. However, these protective layers deform and degrade over time. For this reason, various tests (hardness, gloss, color, adhesion, roughness, *etc*.) are carried out by paint/varnish manufacturers in order to determine the pre-marketing performance of the protective layers on various material surfaces. In addition, before these tests, protective layers are exposed to external environmental conditions and natural or artificial aging processes such as rain water or snow water effect, sun rays, accelerated aging, salt corrosion, abrasion, scrubbing, and household chemicals, and various deformations occur on protective layers (Rutherford *et al.* 1997; Cayton and Sawitowski 2005; Shi *et al.* 2011).

Today, conventional scrub tests are used to determine the resistance of protective layers such as paint and varnish on various sample surfaces against household chemicals (Redsve *et al.* 2003; Fitzner and Aßmus 2005; Kok and Young 2014; Martinez *et al.* 2014).

In a previous study, Redsve *et al.* (2003) performed a cleanability test on ceramic tile material with an Erichsen scrub tester. The researchers used a microfiber mop and two different chemicals during the scrubbing process. They calculated the cleanability time of the ceramic material with a stopwatch. Kok and Young (2014) performed a wet scrub test to test the cleanability of the insect residue adhering to the paint and coating layer on the aircraft wing. A Zeiss LSM 710 confocal laser scanning microscope was used to measure the insect residue left on the surfaces after scrub and the change in the coating film layer. They also obtained data by weighing the weights of the experimental samples. Marco *et al.* (2015) used 37 scrub cycles per minute, 135 g weight, and 3M Scotch Brite 7448 abrasive pads on the glass panel material surface according to the principles of ISO 11998 standard and performed 500 scrub cycles. They used scanning electron microscopy (SEM) to investigate the changes in the surface of the glass panel samples. Santos *et al.* (2019) used a Leneta wet scrub tester to examine the dirt holding status of water-based paints. They used a BYK color measuring device to reveal the color differences between the control samples and the dirty paint layer. Helwani *et al.* (2021) used a BGD 526 wet scrub tester to test the gloss and washability of polyvinyl acetate (PVAc) paint. Then, they used the luminance device according to the Indonesian standard SNI 3564:2009 to measure the brightness of the samples.

When the studies conducted with traditional scrub testers were reviewed, it was seen that researchers had to measure the abrasion changes that occurred after scrubbing on the sample surfaces using different test devices (balance, color and gloss device, SEM, *etc*.).

Unlike traditional scrub testers, an Image Processing Based Scrub Tester (IPBST) designed and produced with the support of TUBİTAK - 221O551 project was used in this study. With the help of this tester, the retinex model was used to detect the abrasion changes that occurred on the sample surfaces after scrubbing with various household chemicals. In color image applications, unwanted light and weather conditions cause brightness in the images. Images without insufficient or uneven lighting are accompanied by low brightness, poor contrast, blurred local details, poor color quality, sudden changes in light, and often too much noise. In the retinex theory, which has taken its place among the techniques for improving low-light images, the image is presented as a product of lighting and reflection. In retinex-based algorithms, the improved image is generally obtained by estimating the lighting component from the input image and then taking the reflection component. The single-scale retinex (SSR) and multi-scale retinex (MSR) algorithms use local Gaussian filters to separate the lighting and reflection components (Rahman *et al.* 1996; Jobson *et al.* 1997b). However, artificial light rings or light circles and color distortion problems have been encountered when applying these algorithms. In multi-scale retinex with color restoration (MSRCR) carried out in the same years, a color restoration function was added to the MSR technique in order to achieve a good color representation in images (Jobson *et al.* 1997a). Michael and Wang (2011) used a Bregman method and proposed a total variation model that allows the separation of the reflection component. The side effect of the logarithmic function of the reflection component restoration resulted in excessive smoothing and loss of fine details. In the later years, Fu *et al.* (2015) proposed a probability-based method that can make simultaneous projection and lighting estimation on the linear plane and preserve details better than the logarithmic plane. In the study titled Multi-scale Fusion Enhancing Method (MF) by Fu *et al.* (2016), three different inputs were obtained for the fusion process by taking the maximum value from the three-color channels. Chromatic contrast weights were used to determine the ratio of these three inputs. In the

final process, the obtained lighting output was combined with the reflection component to obtain an improved image. In the retinex model, which is called the Joint Intrinsic-Extrinsic Prior Model (JieP) and which was presented in 2017, lighting and reflection in the linear space can be differentiated at the same time. In the first part of the study, the aim was to preserve the structure within the intrinsic characteristics with the feature called local variation deviation (Cai *et al.* 2017). The most important feature of the study proposed by Li *et al.* (2018) is that it makes noise-free lighting predictions using the reflection and alternative optimization function that simultaneously reveals the structure. Xu *et al.* (2020a) performed the improvement process by generating structure and texture mapping using exponential local derivatives. For this purpose, the Exponentiated Mean Local Variance (EMLV) was first proposed for flexible structure and texture prediction. The solution of this model, which they called Structure and Texture Aware Retinex (STAR), was carried out with an alternative optimization algorithm converted to vectorized least squares regression. In another study conducted in recent years, one of the main purposes of the retinex-based variational models proposed by Ma *et al.* (2022) was to create a noise-free image. After reconstructing the reflection and lighting components with the fractional derivative of the image, a simple constraint application was performed. Second, a weighted correction process that can eliminate noise with an adaptive texture map was presented.

The measurement or estimation of abrasion that occurs on sample surfaces as a result of the scrubbing process is difficult due to the two-dimensionality of the images. However, it is possible to obtain information about the surface textures of the samples by estimating the light reflecting property of the surface. Therefore, this study aimed to obtain indirect information about the abrasion that occurred on the sample surfaces after scrubbing by using a retinex-based method. First, retinex-based methods used in the improvement of low-light color images from the nineties to the present were examined. The JieP method was used to separate lighting and reflection components in images. The plan was to produce a new device that is suitable for industry 4.0 level, that can use the methods of automation, robotic arm, computer, and digital transformation, and that utilizes flaw detection software and artificial intelligence detecting defects at every repetition and presenting digital data, in order to perform image processing-based abrasion measurement (Çark 2020; Duman and Özsoy 2021; Erten and Göktepeliler 2022; Karamustafa *et al.* 2022). Based on this plan, the IPBST was designed and produced in order to obtain a report after the scrubbing process, which is the most important deficiency in the existing scrub testers. The degree of abrasion occurring on the sample surfaces with protective layers after the scrubbing process can be determined, and the evaluation errors arising from the individual perception differences can be eliminated. As the degree of image processing-based abrasion can be determined without using a different tester to measure the amount of abrasion, an innovative and original contribution can be made in terms of reducing manpower and saving time and equipment. Increasing occupational safety and ease of use thanks to remote sensing makes this metric a new and widely used abrasion measurement metric.

EXPERIMENTAL

Preparation of Samples

First class, 8 mm thick, bright white, high gloss acrylic coated MDF, PVC coated MDF, MDF ready-to-use lam sheets, and raw MDF sheets, which are widely used in the furniture industry, were used. The samples with 520×310 mm dimensions were kept in an

air-conditioning cabinet at 23±2 °C and 50±3% relative humidity, according to the principles specified in Turkish Standard (TS) EN 322 (1999), until they reached a constant weight, and their moisture content was reduced to 9 to 10% (Fig. 1a). A protective layer was applied to all raw MDF boards by applying glossy white cellulosic, polyurethane, acrylic and water-based lacquer paint to the surfaces of the raw MDF panels in accordance with the American Society for Testing and Materials Standard (ASTM) D 3023 (1998) (Fig. 1b) (Budakçı 2003; ASTM D3023-98, 2017; DYO 2023). Then, these lacquered samples were first allowed to reach 9 to 10% moisture content in the room conditions (Fig. 1c) and then in the air-conditioning cabinet (Fig. 1d).

Fig. 1. (a) Conditioning of samples, (**b)** Application of lacquer paint on raw MDF surfaces, **(c)** Drying of painted samples at room conditions, **(d)** Conditioning of the lacquered painted samples

WTP and UV printing processes, which are decorative coating types that have been increasingly used in recent years, were applied to the surfaces of the samples. In the WTP process, the self-pool automatic immersion device was designed, manufactured, and used (Fig. 2a). With the help of this device, 30 µm thick PVAc-based carbon fiber patterned WTP film was coated on the sample panel surfaces using 45º dipping angle, 100 cm/min dipping speed, and 5 to 10 s dipping parameters (Kaçamer and Budakçı 2023). The UV printing machine used in the glass coating industry was used for the UV printing process. Before UV printing, carbon pattern work was performed in Adobe Photoshop program (Fig. 2b) (Kurniawan and Lubis 2022; Adobe 2023). During the UV printing process, the movement speed of the ink ejection head was set at 52 m/min; the UV curing lamp was set at 1000 w Hg (mercury), and the distance between the sample panel surface and the nozzle was set as 3 mm. Spraying the UV paint with the nozzle and the UV curing lamp were operated simultaneously during printing. After these adjustments, UV printing was applied to the surfaces of the sample panels (Fig. 2c).

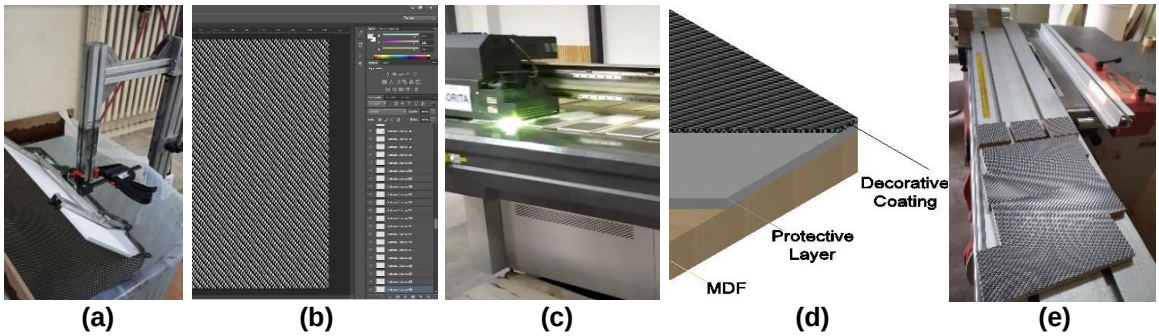

Fig. 2. (a) WTP process, **(b)** Carbon pattern design, **(c)** UV printing, **(d)** WTP coated sample plates, **(e)** Cutting of WTP and UV printed samples.

WTP and UV-printed samples (Fig. 2d), which are modern decorative coating types, were cut in 100×100 mm (Fig. 2e). A total of 840 samples were prepared for 84 different groups, each containing two independent measurement methods.

Image Processing Based Scrub Tester (IPBST)

The IPBST was designed and produced with the project support of the Scientific and Technological Research Council of Turkey (TUBITAK)-221O551 in order to test the resistance of WTP and UV printed sample panels to household chemicals and to measure the abrasion changes on the surfaces of the sample panels using the image processing technique (Fig. 3). A calibration certificate was obtained from the Turkish Standards Institute, Directorate of Ankara-Ostim Laboratories according to the TS EN ISO 11998:2006E standard in order to certify the working accuracy of the produced device.

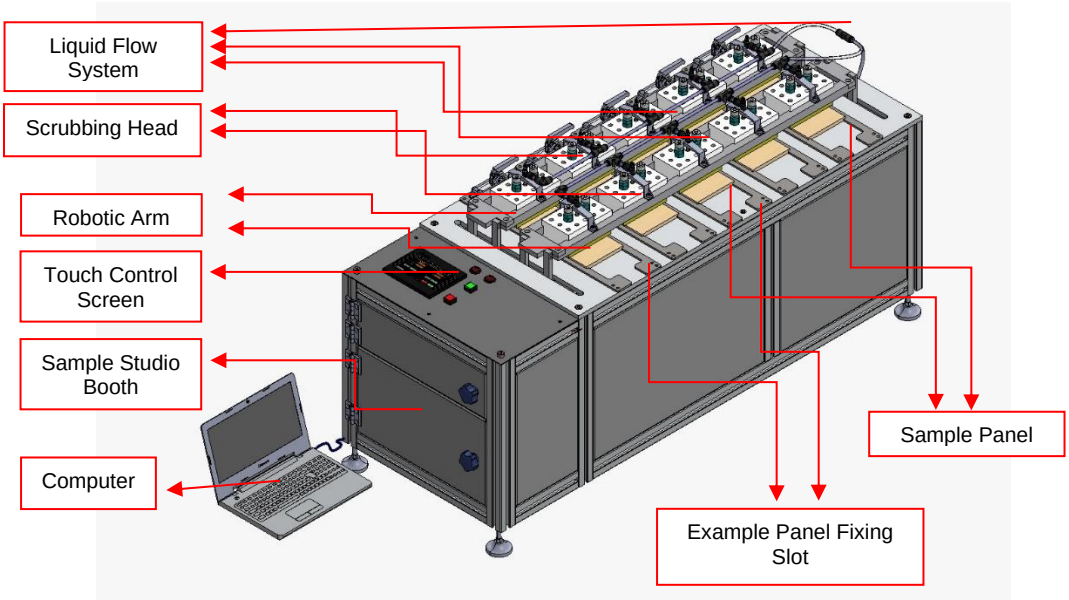

Fig. 3. Image Processing Based Scrub Tester (IPBST) prototype

Digital images of the studio cabinet integrated into the device and of the sample panels were taken before the scrubbing process. These samples were then exposed to various household chemicals with the IPBST. During the operation of the device, a 135±1 g scrubbing head unit contacted the coated surfaces of the samples according to the principles specified in the TS EN ISO 11998 (2006) standard. 3M Scotch Brite sponge pad was used as a scrubbing pad. The scrubbing heads performed the scrubbing process by making cycles in the +Z and –Z axis with a total of 200 smooth linear movements, 37±2 times per minute. Ethyl alcohol, acetone, bleach, liquid dishwashing liquid, lemon juice and cola were selected as scrubbing chemicals from among household chemicals according to the ASTM D1308-20 (2020) standard, and 5 mL of these chemicals was applied to the surface of each sample (Fig. 4).

After the scrubbing process with the IPBST using various household chemicals, digital images of each sample were recorded. The amount of abrasion that occurred on WTP and UV printed samples as a result of the scrubbing process was obtained with a stereo microscope device and the image processing-based abrasion measurement method proposed in this study.

Fig. 4. Scrubbing with dishwashing liquid in IPBST

Abrasion Measurement with Stereo Microscope

The stereo microscope device and the abrasion measurement method, which are frequently used in the literature, were utilized in order to test and compare the abrasion measurement accuracy of the IPBST. The 2 mm thick test samples were prepared from the body of the scrubbed samples and from the unrubbed control samples in the IPBST (Fig. 5a). A Zeiss Axio Scope A1 stereo microscope and the camera system attached to it were used to measure the coating thicknesses in the sample section (Fig. 5b) (Çiftçi *et al.* 2021). Digital images were taken by looking at the coating film thickness on the section surface from a 10x lens measurement unit (Fig. 5c). The same device and the ZEN software program on the computer connected to it were used to take the images of the samples and measure the coating film thickness, and the thickness values of the coating film were measured with micron (μm) precision (İzzetoğlu *et al.* 2021).

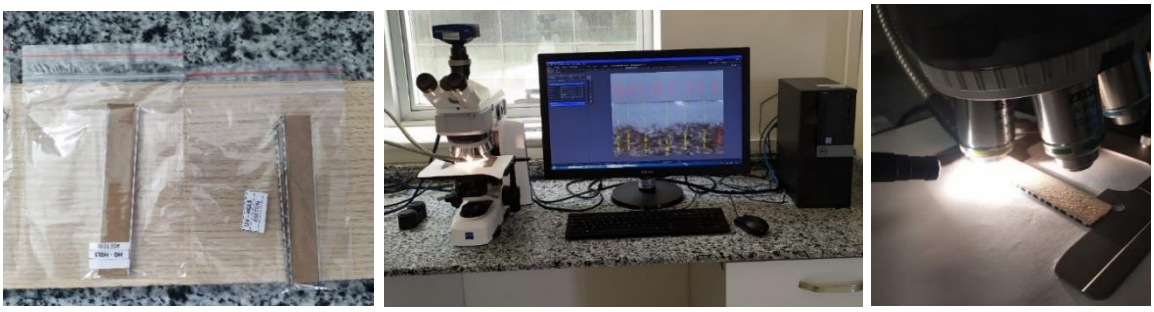

(a) **b)** **(c)**

Fig. 5. (a) Preparation of sample sections from the panels, **(b)** Measurement of coating film thicknesses with a stereo microscope, **(c)** Examination with 10x lens measurement unit

The coating film thickness (cells) of all samples were measured before scrubbing (Fig. 6a) and after scrubbing (Fig. 6b) according to the ASTM E112 (2013) standard on the images obtained from the stereo microscope device (Fig. 6b). At least 5 coating film thickness measurements were taken from each sample image section. It took an average of 18 min to measure each sample.

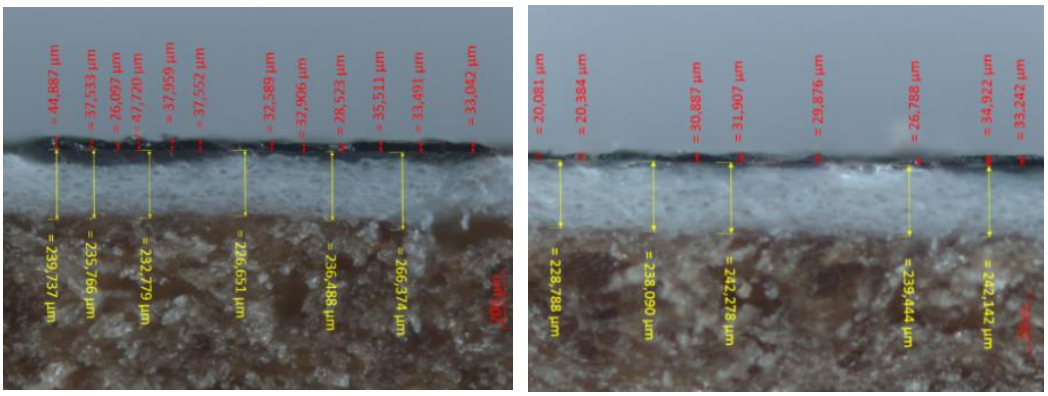

(a) **(b)**

Fig. 6. (a) Coating film thickness measurement of UV-coated MDF Lam sample before abrasion, **(b)** Coating film thickness measurement of the same sample after scrubbing with bleach

Joint Intrinsic-Extrinsic Prior Retinex Model

The retinex theory, which is widely used for the improvement of low-light color images, generally analyzes local image derivatives and separates the image into lighting and reflection components. It was first proposed by Land and McCann in 1971, and the word retinex was formed by synthesizing two words, retina and cortex. Figure 7 shows the symbolic representation of the lighting and reflection components of an image, which consists of two separate components (Katırcıoğlu 2021). By using the retinex method, it is aimed to obtain information about the sample surface by comparing the reflection component images of the samples before and after brushing. In this process, the lighting component is assumed to be constant before and after each brushing. This assumption makes sense if the light source, camera calibration, lens settings, and environmental conditions in the cabin are the same.

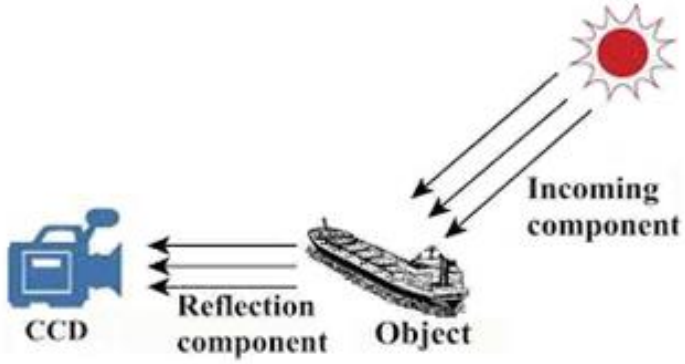

Fig. 7. Symbolic representation of the retinex model

Lighting and reflection can be separated simultaneously in a linear space in the intrinsic and extrinsic priority retinex model presented by Xu *et al.* in 2020b. In the first part of the study, the aim was to protect the structure in the internal characteristics, with the feature called local variation deviation.

$$R_{x/y} = \left| \frac{\nabla_{x/y} I}{\frac{1}{|\Omega|} \sum_{\Omega} \nabla_{x/y} I + \varepsilon} \right| \quad (1)$$

In the local variation deviation given in Equation (1), $\nabla_{x/y}$ represents the slope operator and Ω represents the local part taken from the image, which is 3x3 in size. Also, ε is a small number used to avoid division by zero (Cai *et al.* 2017).

Algorithm 1. A Joint Intrinsic-Extrinsic Prior Model

Input: observed image S, parameters α, β and λ, maximum iterations K and stopping parameters ε.
Output: lighting I and reflectance R.

initialize $I_0 \leftarrow S_2$:
for k = 1 to K **do**
  compute weights $u_{x/y}$ in Eq. (2)
  update I_k using (3)
    if k = 1 **then**
      $R_0 = S/I_1$
    end if
  compute weights $v_{x/y}$ in Eq. (2)
  update R_k using (4)
    if $||I_k - I_{k-1}||/||I_{k-1}|| \leq \varepsilon$ or $||R_k - R_{k-1}||/||R_{k-1}|| \leq \varepsilon$ **then**
      break
    end if
end for.

According to Eq. 2, as given in Algorithm 1, $u_{x/y}$ weight values are calculated for lighting and $v_{x/y}$ values are calculated for reflection. The reflection I_1 in the first iteration is calculated according to Equation (3).

$$\begin{cases} u_{x/y} = \left(\left| \frac{1}{\Omega} \Sigma_{\Omega} \nabla_{x/y} I \right| |\nabla_{x/y} I| + \varepsilon \right)^{-1} \\ v_{x/y} = \left(|\nabla_{x/y} R| + \varepsilon \right)^{-1} \end{cases} \quad (2)$$

$$(P1) I_k = argmin \|I.R_{k-1} - S\|_2^2 + \alpha \left(u_x \|\nabla_x I\|_2^2 + u_y \left\|\nabla_y I\right\|_2^2 \right) + \lambda \|I - B\|_2^2 \quad (3)$$

where S is the original input image, B is the bright channel, and $\max_{\Omega} \left(\max_{c \in \{r,g,b\}} S^c \right)$ is the maximum color value of the received image particle. R_1 is updated using Equation (4) after the initial value of reflection, R_0, is found in the first iteration.

$$(P2) R_k = argmin \|I_k.R - S\|_2^2 + \beta \left(v_x \|\nabla_x R\|_2^2 + v_y \left\|\nabla_y R\right\|_2^2 \right)$$
$$R_k = (I_k^T I_k + \beta N_k)^{-1} (I_k^T S) \quad (4)$$

The optimization process for image enhancement ends when the condition in Algorithm 1 is fulfilled. The I_k (Lighting) and R_k (Reflection) images in the last iteration are obtained.

Method: Image Processing Based Abrasion Measurement

This study aimed to obtain information about the amount of abrasion that occurs on the sample surfaces after scrubbing. First, images of the samples were taken before and after scrubbing in the IPBST. In these two images, the background image parts, which contain the undesired samples to be processed, were cut automatically and prepared for analysis.

Then, the lighting and reflection components of the images were obtained with the retinex model, using the V intensity channel of the HSV color space for both images. JieP, which is widely used in the literature, was selected for this separation process.

Only reflection components of both images were used in the study. According to the Retinex model, the lighting components are considered equal, since the environmental conditions, the camera's shooting angle, the lens setting, and the light intensity are the same in the imaging cabinet. The reflection components of the images taken before and after scrubbing were normalized. The pixel values of the projection images are rescaled between [0,1] so that all values have a positive scale. Equations (5) and (6) present the normalization process for both reflection images.

$$R_{new\_ab} = \frac{R_{ab} - R_{ab\_min}}{R_{ab\_max} - R_{ab\_min}} \quad (5)$$

$$R_{new\_aa} = \frac{R_{aa} - R_{aa\_min}}{R_{aa\_max} - R_{aa\_min}} \quad (6)$$

R_{new_ab} in Eq. 5 and R_{new_aa} in Eq. 6 represent reflection component images after normalization using abrasion before (ab) and abrasion after (aa) sub-indices.

$$A_d = \sum_{i=0}^{M} \sum_{j=0}^{N} \left| R_{new_{ab}-ij} - R_{new_{aa}-ij} \right| \quad (7)$$

$$T_{aa} = \sum_{i=0}^{M} \sum_{j=0}^{N} R_{new_{ab}-ij} \quad (8)$$

The sum of the differences of the two reflection components in Eq. 7 is expressed as A_d, and the sum of the pixel values of the original reflection component before scrubbing is expressed as T_{aa} in Eq. 8. M and N are the dimensions of the projection component images, and the dimensions of the two images must be the same.

$$A = \frac{A_d}{T_{aa}} * 100 \quad (9)$$

Abrasion measurement was performed by dividing the sum of the differences by the original image values to find the *A* value.

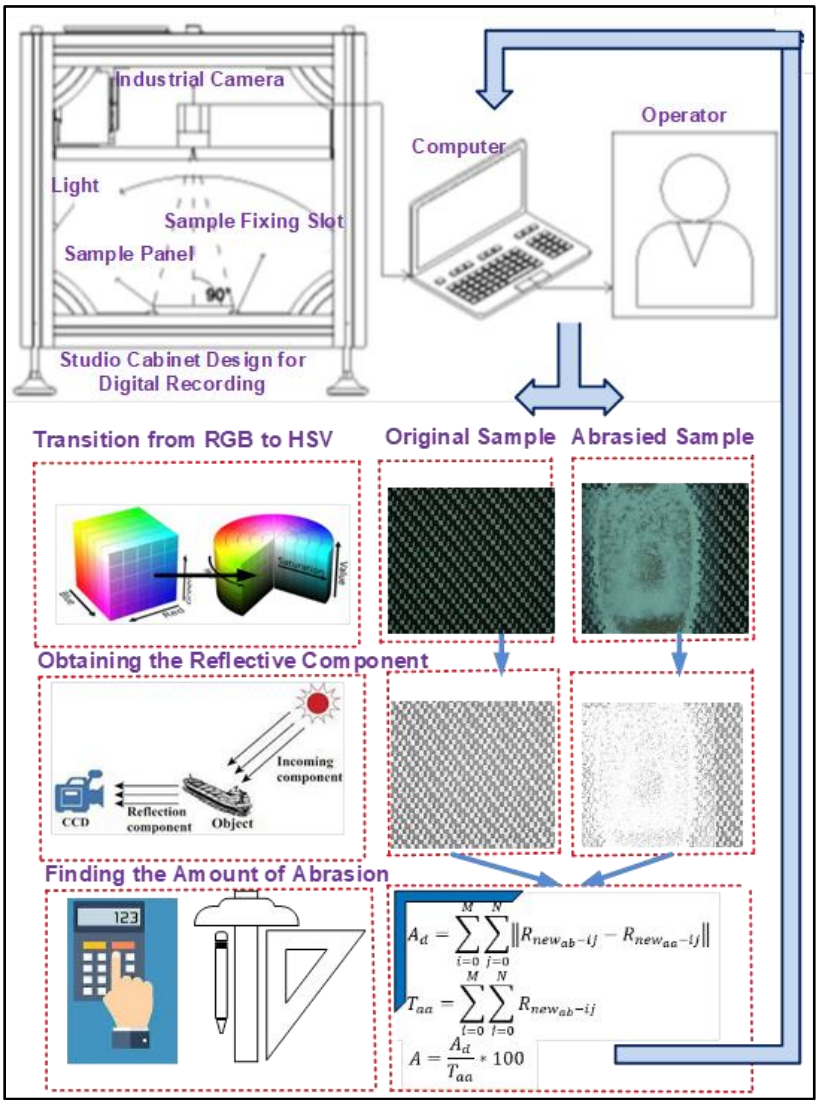

Fig. 8. Flowchart of the proposed Retinex-based abrasion measurement

The flow chart of the proposed system is given in Fig. 8. First, images before and after scrubbing were taken from the scrub tester. After cutting the background image with the apparatus holding the samples in the imaging cabinet, both images were converted to HSV color space. Reflection and lighting components were obtained using the V channel Algorithm 1 of the HSV color space. Finally, the amount of abrasion change was determined using the two reflection component images and Eqs. 5, 6, 7, 8, and 9.

The amount of abrasion change was determined using the Matlab Graphical User Interface (GUI), and its general view is given in Fig. 9 (MathWorks, 2023). First, the sample was placed in the imaging cabinet before entering the IPBST, and its image was taken and recorded. After the scrubbing process is finished, the same sample is taken to the cabinet again and the degradation was captured and saved with the “TAKE IMAGE” and “SAVE” buttons. The program starts to run when the user presses the "START" button after opening the images of the samples whose amount of abrasion he wants to measure from the file. The results of the method are given at the bottom right of the interface. The amount of abrasion is presented numerically and verbally in percentage with the images of the reflection component. It took an average of 2 min to measure each sample.

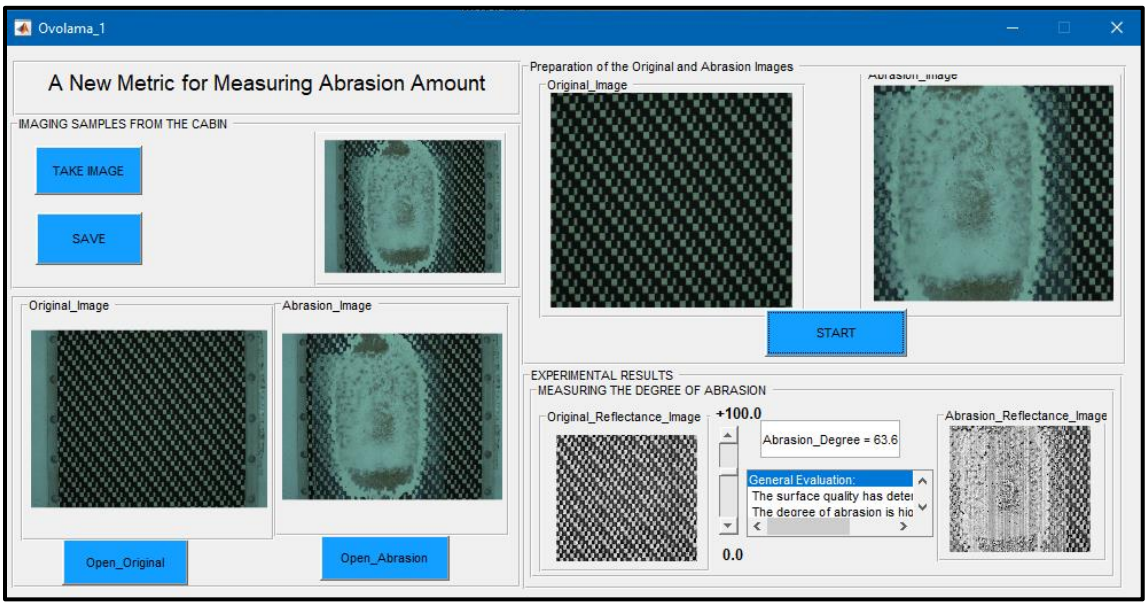

Fig. 9. Matlab GUI interface of the proposed Retinex based abrasion measurement

RESULTS AND DISCUSSION

The CoStat and SPSS 24 statistical package program (IBM Corp., Armonk, NY) was used to analyze the data gathered in this study (IBM, 2021; Costat 2023). The effects of measuring protective layer type, decorative coating type, household chemical type, and type of abrasion measurement and the interactions of each sample on these factors, were determined using multivariate analysis of variance (ANOVA) test. Comparisons were applied by using Duncan's multiple range test (DMRT) and least significant difference (LSD) critical values, while the factors causing the differences were examined as well.

Multiple Analysis of Variance (ANOVA) Test Results

Scrubbing was carried out to determine the resistance of WTP and UV printed samples to household chemicals using the IPBST. The arithmetic averages of the abrasion that occurred on the coating film layer as a result of the scrubbing process were found to be different according to the factors of abrasion measurement method, decorative coating type, type of protective layer, and household chemical type. The ANOVA test was performed to determine the factor that caused this difference, and the results are given in Table 1.

The ANOVA analysis revealed that (Table 1) all factors and interactions affected the abrasion measurement values ($P \leq 0.05$). The Duncan's multiple range test (DMRT) comparison results performed using the LSD critical value for the factors of abrasion measurement method, decorative coating type, protective layer type and household chemical type are given in Table 2.

Table 1. The Results of the ANOVA Pertaining to Abrasion Measurements

Factors	Degrees of Freedom	Sum of Squares	Mean Square	F Value	Level of Significance
Abrasion Measurement Method (A)	1	15221.209	15221.209	203.402	0.000*
Protective Layer Type (B)	6	29164.449	4860.742	64.954	0.000*
Decorative Coating Type (C)	6	7358.255	1226.376	16.388	0.000*
Household Chemical Type (D)	1	24574.248	24574.248	328.387	0.000*
Interaction (AB)	1	4421.832	4421.832	59.089	0.000*
Interaction (AC)	6	26975.013	4495.836	60.078	0.000*
Interaction (AD)	6	3050.373	508.395	6.794	0.000*
Interaction (BC)	5	317323.665	63464.733	848.082	0.000*
Interaction (BD)	5	31424.497	6284.899	83.985	0.000*
Interaction (CD)	30	44358.217	1478.607	19.759	0.000*
Interaction (ABC)	30	10286.802	342.893	4.582	0.000*
Interaction (ABD)	5	74283.025	14856.605	198.529	0.000*
Interaction (ACD)	5	14269.620	2853.924	38.137	0.000*
Interaction (BCD)	30	74406.331	2480.211	33.143	0.000*
Interaction (ABCD)	30	13951.623	465.054	6.215	0.000*
Error	1512	113147.920	74.833		
Total	1679	804217.078			
*Note: *Significant at 95% confidence level*					

Table 2. DMRT Results Pertaining to the Factors of Abrasion Measurement Method, Decorative Coating Type, Protective Layer Type and Household Chemical Type (%)

Abrasion Measurement Method	$\bar{x}$	***HG***	LSD
Zeiss Axio Scope A1 Stereo Microscope	34.7	A*	± 0.827
Image Processing Based Abrasion Measurement	28.7	B	
Decorative Coating Type	$\bar{x}$	***HG***	LSD
Water Transfer Printing (WTP)	35.5	A*	± 0.827
UV Printing	27.9	B	
Protective Layer Type	$\bar{x}$	***HG***	LSD
Cellulosic Lacquer Painted Sample	37.9	A	± 1.549
Polyurethane Lacquer Painted Sample	30.5	B	
Acrylic Lacquer Painted Sample	28.6	CD	
Water Based Lacquer Painted Sample	29.4	BC	
MDF Lam Sample	29.8	BC	
High Gloss Acrylic MDF Sample	27.4	D	
PVC MDF Sample	38.4	A*	
Household Chemical Type	$\bar{x}$	***HG***	LSD
Acetone	62.3	A*	± 1.434
Alcohol	25.1	CD	
Bleach	26.7	BC	
Dishwashing Liquid	24.4	DE	
Lemon juice	23.9	EF	
Coke	28.0	B	
*Note: $\bar{x}$: Arithmetic mean; HG: homogeneity group; * :the highest abrasion value*			

In the abrasion measurement method, the highest abrasion amount (34.7%) was obtained with Zeiss Axio Scope A1 stereo microscope, and the lowest amount (28.7%) was obtained with the image processing-based abrasion measurement method. As for the decorative coating type, the highest abrasion amount was obtained in WTP samples (35.5%), while the lowest amount was observed in UV printed samples (27.9%). The highest abrasion amount was observed in the PVC MDF panel samples (38.4%), while the lowest amount was found in high gloss acrylic MDF samples (27.4%) in the factor of protective layer type. As for the level of household chemical, the highest abrasion amount was found in the samples that were scrubbed with acetone (62.3%), while the lowest amount was obtained in samples that were scrubbed with lemon juice (23.9%).

This data further indicates that WTP and UV printing on the surface of high gloss acrylic MDF panel samples show the best resistance to household chemicals compared to other sample types. The UV printing showed better resistance to household chemicals than the WTP. It was seen that the household chemical causing the highest level of abrasion in the WTP and UV printed samples was acetone, and the chemical causing the lowest level of abrasion was lemon juice.

DMRT Comparison Data Obtained with the Stereo Microscope and the Image Processing Based Abrasion Measurement Method

Table 3 shows the results of the Zeiss Axio Scope A1 stereo microscope and the DMRT comparison performed to determine the difference between the abrasion values for the factors of measurement methods, protective layer type, decorative coating type and household chemical type obtained using the image processing-based abrasion measurement method within the IPBST.

Table 3. DMRT Results Pertaining to the Difference Between the Abrasion Rates Across the Factors of Measurement Methods, Protective Layer Type, Decorative Coating Type, and Household Chemical Type (%)

Protective Layer Type	Decorative Coating Type	Household Chemical Type	Measurement Methods			
			IPBST		Stereo Microscope	
			$\bar{x}$	HG	$\bar{x}$	HG
Cellulosic Lacquer Painted Sample	WTP	Acetone	54.9	DE	99.9	**A***
		Alcohol	23.6	&e-zA-E	31.2	L-Za-e
		Bleach	24.1	&e-zA-C	36.5	I-O
		Dishwashing	28.8	P-Za-l	43.6	F-I
		Lemon juice	23.9	&e-zA-D	31.8	K-Za-d
		Coke	21.1	&m-zA-J	25.6	&c-x
	UV Printing	Acetone	69.0	B	99.9	**A***
		Alcohol	25.4	&c-y	30.3	L-Za-f
		Bleach	28.2	R-Za-o	37.1	İ-N
		Dishwashing	17.9	&y-zA-N	19.9	&r-zA-L
		Lemon juice	21.7	&k-zA-H	23.2	&f-zA-F
		Coke	46.9	E-G	43.7	F-I
Polyurethane Lacquer	WTP	Acetone	65.1	BC	99.9	**A***
		Alcohol	16.2	&&E-Q	14.3	&&H-R
		Bleach	28.8	Q-Za-l	35.7	J-S
		Dishwashing	22.0	&h-zA-G	28.0	T-Za-o
		Lemon juice	25.5	&c-y	32.0	K-Za-c
		Coke	26.3	&a-w	34.1	J-Z
	UV	Acetone	26.8	X-Za-t	35.5	J-T
		Alcohol	25.4	&c-y	29.5	O-Za-h

Painted Sample	Printing	Bleach	21.9	&h-zA-G	26.6	Za-u
		Dishwashing	24.6	&c-zAB	27.5	V-Za-r
		Lemon juice	22.9	&f-zA-F	25.8	&c-x
		Coke	18.7	&x-zA-M	17.7	&&A-O
Acrylic Lacquer Painted Sample	WTP	Acetone	59.0	CD	99.9	**A***
		Alcohol	21.9	&ı-zA-H	21.8	&j-zA-H
		Bleach	17.4	&&A-O	9.4	&&P-T
		Dishwashing	25.1	&c-z	27.1	W-Za-s
		Lemon juice	27.8	U-Za-q	36.2	I-Q
		Coke	33.6	J-Za	40.7	G-J
	UV Printing	Acetone	21.3	&l-zA-I	16.5	&&C-P
		Alcohol	24.1	&e-zA-C	35.8	J-R
		Bleach	26.7	YZa-u	47.5	E-G
		Dishwashing	16.4	&&D-Q	11.9	&&M-S
		Lemon juice	18.6	&x-zA-M	13.0	&&L-R
		Coke	19.7	&s-zA-L	15.1	&&G-Q
Water Based Lacquer Painted Sample	WTP	Acetone	59.1	CD	99.9	**A***
		Alcohol	16.2	&&E-Q	10.3	&&O-T
		Bleach	24.3	&d-zAB	29.3	O-Za-i
		Dishwashing	20.7	&o-zA-K	16.0	&&F-Q
		Lemon juice	23.6	&e-zA-E	28.6	R-Za-m
		Coke	28.7	Q-Za-m	35.3	J-U
	UV Printing	Acetone	34.5	J-W	43.4	F-I
		Alcohol	28.2	S-Za-o	29.3	O-Za-j
		Bleach	18.9	&v-zA-M	22.2	&h-zA-G
		Dishwashing	20.9	&r-zA-L	23.9	&e-zA-D
		Lemon juice	19.4	&t-zA-M	22.9	&f-zA-F
		Coke	22.9	&f-zA-F	28.5	R-Za-n
MDF Lam Sample	WTP	Acetone	58.7	CD	99.9	**A***
		Alcohol	28.1	T-Za-o	20.0	&r-zA-L
		Bleach	24.3	&d-zAB	50.6	EF
		Dishwashing	18.8	&w-zA-M	25.8	&c-x
		Lemon juice	25.5	&c-x	29.4	O-Za-i
		Coke	20.2	&q-zA-L	40.5	G-J
	UV Printing	Acetone	20.3	&p-zA-L	13.2	&&K-R
		Alcohol	24.3	&d-zAB	17.5	&&A-O
		Bleach	27.2	W-Za-s	21.9	&ı-zA-G
		Dishwashing	34.9	J-V	60.9	CD
		Lemon juice	17.0	&&B-O	7.1	&&R-T
		Coke	19.2	&u-zA-M	8.9	&&Q-T
High Gloss Acrylic MDF Sample	WTP	Acetone	64.3	BC	99.9	**A***
		Alcohol	31.1	L-Za-e	23.1	&f-zA-F
		Bleach	24.8	&c-zA	30.3	M-Za-g
		Dishwashing	33.6	J-Zab	22.4	&h-zA-G
		Lemon juice	28.3	R-Za-n	22.7	&g-zA-F
		Coke	34.3	J-X	18.7	&x-zA-M
	UV Printing	Acetone	30.9	L-Za-e	39.7	H-J
		Alcohol	20.9	&n-zA-J	13.6	&&J-R
		Bleach	17.4	&&A-O	4.4	&&ST
		Dishwashing	13.2	&&K-R	3.3	&&T
		Lemon juice	22.3	&h-zA-G	9.3	&&P-T
		Coke	26.0	&b-x	23.1	&f-zA-F
PVC MDF	WTP	Acetone	59.9	CD	99.9	**A***
		Alcohol	26.4	&a-v	27.9	T-Za-p
		Bleach	30.2	N-Za-g	14.1	&&IJ-R
		Dishwashing	25.1	&cd-z	10.4	&&N-T
		Lemon juice	19.9	&r-zA-L	47.2	FG
		Coke	26.5	&a-v	36.4	I-P

Sample	UV Printing	Acetone	71.8	B	99.9	**A***
		Alcohol	37.8	I-M	47.9	E-G
		Bleach	28.9	O-Za-k	37.9	IJ-L
		Dishwashing	25.9	&c-x	34.3	J-Y
		Lemon juice	22.9	&f-zA-F	20.3	&p-zA-L
		Coke	31.1	L-Za-e	39.2	I-K
LSD ± 7,588						
*Note: x̄ : Arithmetic mean; HG: homogeneity group; * :the highest abrasion value*						

According to Table 3, the measurements made with the stereo microscope device revealed that the highest abrasion amount (99.9%) was seen in all the samples whose surfaces were first WTP treated and then scrubbed with acetone, and that the WTP film was completely eroded from the sample surfaces. Secondly, when the UV-printed samples were examined, it was seen that the highest abrasion amount (99.9%) was observed on the surfaces of cellulosic lacquer painted samples and PVC MDF samples that were UV printed and then scrubbed with acetone, and the UV printing coating film was completely eroded from the surface of these two panel samples (Fig. 10). The lowest abrasion amount (3.3%) was observed on the surface of high gloss acrylic samples treated with dishwashing liquid after UV printing.

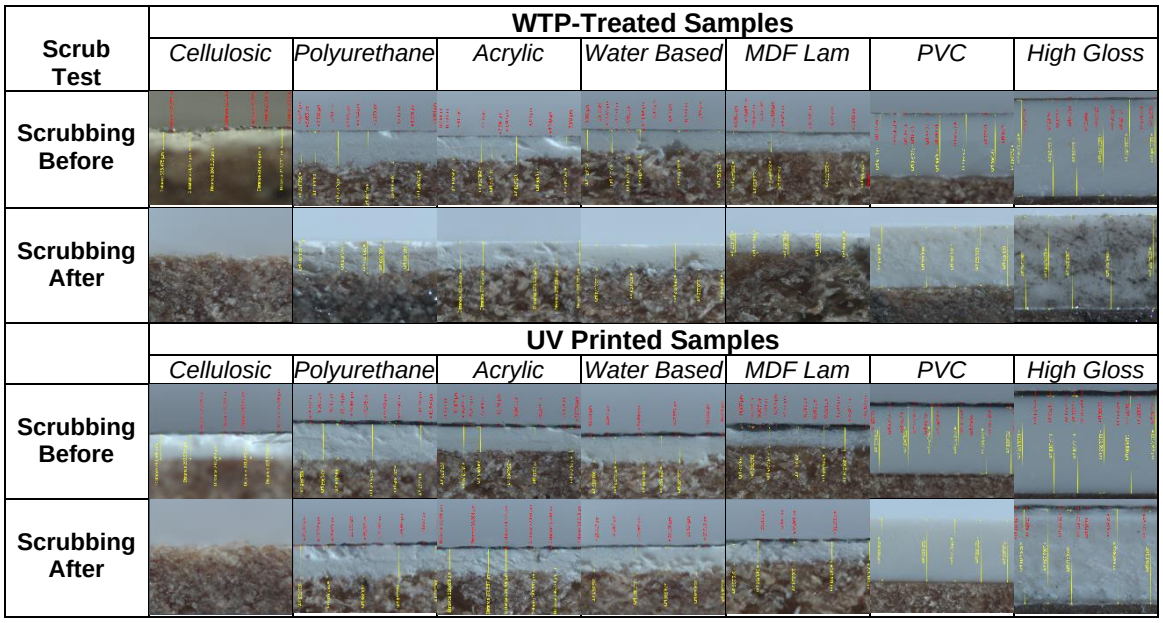

Fig. 10. Measurement of coating thickness (µm) of WTP and UV printed samples with a stereo microscope before and after scrubbing

In Table 3, the first specimens to be considered were those with whole surfaces that had been WTP-treated. The table shows the image processing-based abrasion measurements of the IPBST. The highest abrasion amount (65.1%) was observed in the samples that were scrubbed with acetone after WTP treatment was applied to the polyurethane lacquer painted surfaces. After scrubbing with acetone in other WTP-treated samples, the abrasion amount was found to be 54.9% in cellulosic lacquer painted samples, 59.1% in acrylic lacquer painted samples, 59.1% in water-based lacquer painted samples, 58.7% in MDF lam samples, 64.3% in high gloss acrylic samples, and 59.9% in PVC MDF samples. It was seen that the WTP film structure on the surfaces of these 7 different samples completely degraded (Fig. 11). The highest abrasion rates were observed in the samples

scrubbed with acetone after UV printing on PVC MDF surfaces and in the samples with cellulosic lacquer paint, at 71.8% and 69.0%, respectively. After UV printing on the surfaces of PVC and cellulosic lacquered samples, it was seen that the coating film structure on the surfaces that were scrubbed with acetone completely degraded (Fig. 11). The lowest abrasion amount was found to be 13.2% in the samples that were scrubbed with dishwashing liquid after UV printing on the surface of high gloss acrylic samples.

Scrub Test	WTP-Treated Samples						
	Cellulosic	*Polyurethane*	*Acrylic*	*Water Based*	*MDF Lam*	*PVC*	*High Gloss*
Scrubbing Before							
Scrubbing After	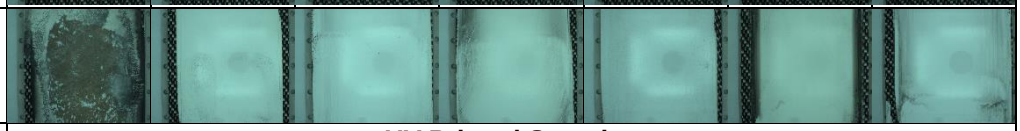						
	UV Printed Samples						
	Cellulosic	*Polyurethane*	*Acrylic*	*Water Based*	*MDF Lam*	*PVC*	*High Gloss*
Scrubbing Before							
Scrubbing After	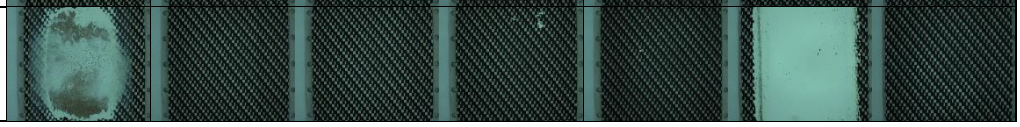						

Fig. 11. Images of WTP and UV printed samples before and after scrubbing

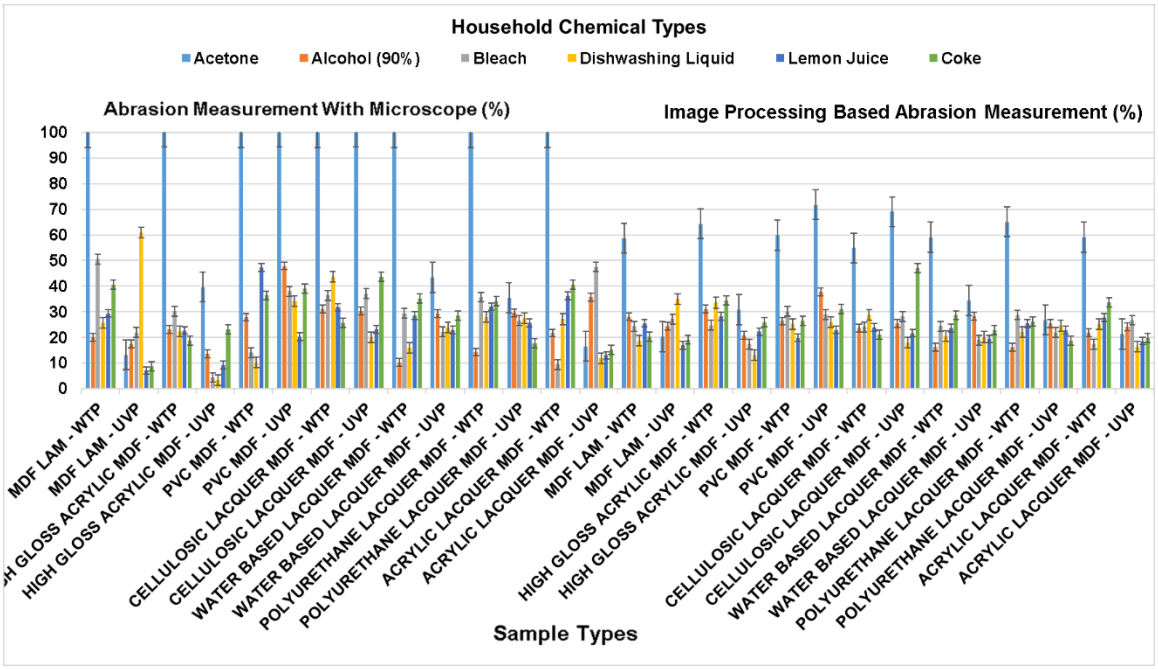

Fig. 12. Intergroup relationships of abrasion amount data obtained by image processing-based abrasion measurement method

When the measurements made with the stereo microscope device were compared with the data obtained using the image processing-based wear measurement method, the highest and lowest wear data obtained from the UV printing and WTP-treated samples showed a strong similarity (Fig. 12).

Correlation Analysis of Abrasion Measurement Methods

Pearson Correlation analysis was performed to reveal the relationship between Zeiss Axio Scope A1 stereo microscope used to measure the abrasion change that occurred on the WTP-treated and UV printed sample surfaces and the abrasion measurement performed with the IPBST as a result of the scrubbing process. The results are given in Table 4.

Table 4. The Relationship Between Zeiss Axio Scope A1 Stereo Microscope and Image Processing-based Abrasion Measurement Method

Pearson Correlation Coefficient (r)	P-Value	Sample Measurement Amount (n)
0,806	0,000*	1680

*: Significant at p<0.01

As seen in Table 4, Pearson correlation analysis showed a statistically strong and significant positive correlation (P<0.01) of 0.81 between two different abrasion measurement methods. This relationship is shown in Fig. 13.

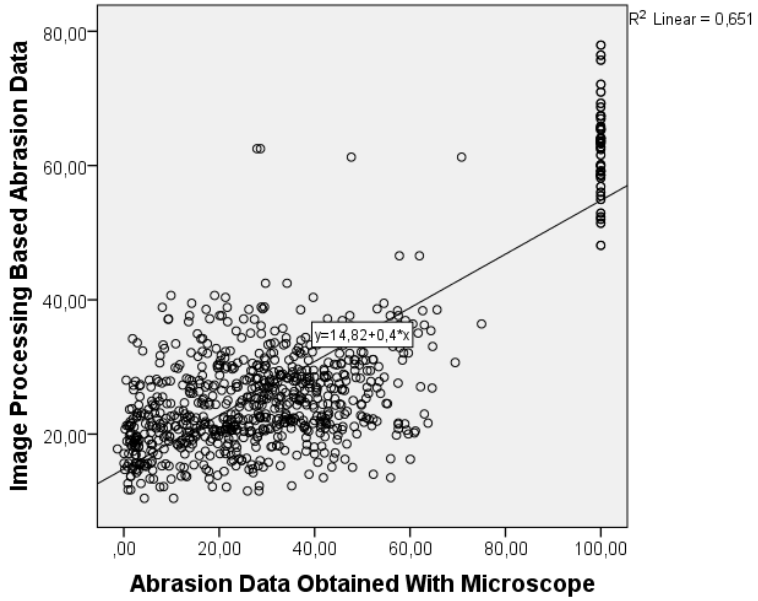

Fig. 13. Correlation between the data obtained from two different abrasion measurement methods.

The correlation graph given in Fig. 13 indicates that the use of the image processing-based abrasion measurement method obtained with the IPBST can be an alternative to the Zeiss Axio Scope A1 stereo microscope.

CONCLUSIONS

1. The highest abrasion value was observed after the WTP-treated surfaces of cellulosic, polyurethane, acrylic, and water-based lacquer painted panels and high gloss acrylic coated MDF, PVC coated MDF, and MDF lam samples were scrubbed with acetone as one of the household chemicals. With the new method proposed in this study, the data obtained by the complete abrasion of the coating film on the sample surfaces (the highest abrasion values) were similar to the measurement data of the microscope device.
2. The lowest abrasion value was measured in high gloss acrylic MDF panel surfaces on which UV printing was applied and then scrubbed with dishwashing liquid. It has been revealed that the lowest abrasion value measurements obtained in the stereo microscope and image processing-based abrasion measurement method used for the detection of abrasion are compatible.
3. It is thought that the reason for the high wear value in the Water Transfer Printing-applied samples is that this coating is produced from water-soluble polyvinyl alcohol (PVAc) material and that household chemicals destroy this coating film structure much more easily.
4. It has been determined that acetone is a much stronger and more effective solvent material than other household chemicals used in the experiments. When the literature is examined, it is seen that acetone is used as a solvent in paint type chemicals. For this reason, it is not recommended to use acetone for cleaning on painted and coated panel surfaces.
5. The relationship between the data obtained using the stereo microscope device and the image processing-based abrasion measurement method was investigated using the Pearson Correlation analysis. It was found that the relationship between both abrasion measurement methods was statistically strong and significant (0.81).
6. The wear measurement made with the image processing technique was 9 times faster than the stereo microscope device. This is an important advantage.
7. Thanks to this method developed to monitor the wear of the coating film, no other test device will be needed. This is a serious cost saver.
8. The image processing-based abrasion measurement method, which is the effective and innovative aspect of the IPBST, can be an alternative to industrial test devices. This method may pave the way for researchers to measure abrasion in a shorter period of time, more effectively, and without using expensive devices.

ACKNOWLEDGMENTS

This study was supported by the project numbered 221O551 within the scope of TUBITAK-1005 National New Ideas and Products Research Support Programme.

REFERENCES CITED

Adobe (2023). "Start with Photoshop. Amazing will follow," (https://www.adobe.com/tr/products/photoshop.html), accessed 01 Jan 2023.

ASTM D 1308-20 (2020). "Standard test method for effect of household chemicals on clear and pigmented coating systems," ASTM International, West Conshohocken, PA, USA.

ASTM D 3023 (1998). "Standard practice for determination of resistance of factory-applied coatings on wood products to stains and reagents," ASTM International, West Conshohocken, PA, USA.

ASTM E112 (2013). "Is there possible bias in ASTM e112 planimetric grain size measurements," ASTM International, West Conshohocken, PA, USA.

Budakci, M. (2003). *Pneumatic Adhesion Test Device Design, Production and Testing in Wood Varnishes*, Ph.D. Dissertation, Gazi University, Ankara, Turkey.

Cai, B., Xu, X., Guo, K., Jia, K., Hu, B., and Tao, D. (2017). "A joint intrinsic-extrinsic prior model for Retinex," in: *Proceedings of the IEEE International Conference on Computer Vision*, pp. 4000-4009.

Çark, Ö. (2020). "The effect of 'internet of things': Technology in the digital transformation process of businesses," *Turkish Studies - Economy* 15(3), 1247-1266. DOI: 10.47644/TurkishStudies.41888

Cayton, R. H., and Sawitowski, T. (2005). "The impact of Nano-materials on coating technologies," in: *Technical Proceedings of the 2005 NSTI Nanotechnology Conference and Trade Show*, Vol. 2, pp. 8-12.

Çiftçi, A., Mollman, R., Yıldırım, H., and Erol, O. (2021). "Observations on some lost crocus taxa of turkey and some thoughts on conservation of wild species," *Bagbahce Journal of Science* 8(3), 47-52.

Costat (2023). "CoStat - Free Statistics Software (for linear, polynomial, multiple, and non-linear regression, nonparametric tests, GLM ANOVA, multiple comparisons of means, analysis of frequency data, correlation, descriptive statistics, *etc*.)," (http://cohortsoftware.com/costat.html), accessed 11 July 2023.

Duman, B., and Özsoy, K. (2022). "A deep learning-based approach for defect detection in powder bed fusion additive manufacturing using transfer learning," *Journal of Gazi University Faculty of Engineering and Architecture* 37(1), 361-376. DOI: 10.17341/gazimmfd.870436

DYO Boya (2022). "Furniture paints," (https://endustriyel.dyo.com.tr/sektorler/mobilya-boyalari/tds-msds-ve-sertifikalar), accessed 18 Oct 2022.

Erten, O., and Göktepeliler, Ö. (2022). "Artificial Intelligence, Machine and Art," *Ankara University Journal of Social Sciences* 13(2), 145-153. DOI: 10.33537/sobild.2022.13.2.13

Fitzner, A., and Aßmus, U. (2005). "Recommendation for the quality assessment of the product performance of all-purpose cleaners," *Söfw Journal* 131(9), 54.

Fu, X., Liao, Y., Zeng, D., Huang, Y., Zhang, X. P., and Ding, X. (2015). "A probabilistic method for image enhancement with simultaneous illumination and reflectance estimation," *IEEE Transactions on Image Processing* 24(12), 4965-4977. DOI: 10.1109/TIP.2015.2474701

Fu, X., Zeng, D., Huang, Y., Liao, Y., Ding, X., and Paisley, J. (2016). "A fusion-based enhancing method for weakly illuminated images," *Signal Processing* 129, 82-96. DOI: 10.1016/j.sigpro.2016.05.031

Helwani, Z., Fadhillah, I., Wiranata, A., and Miharyono, J. (2021). "Opacity and washability properties of emulsion paint with natural rubber latex/polyvinyl acetate blend binder," *Journal of Physics: Conference Series* 2049, 1. DOI: 10.1088/1742-6596/2049/1/012092

IBM (2021). "Downloading IBM SPSS Statistics 24," (https://www.ibm.com/support/pages/downloading-ibm-spss-statistics-24), accessed 11 July 2023.

İzzetoğlu, G. T., Serbestoğlu, İ. N., Özkan, S., and Yalçın, S. (2021). "The comparasion of some AgNOR Parameters of Purkinje cells in the laying and broiler chicks exposed to daily cyclic lighting during the embryonic period," *Kahramanmaraş Sutcu Imam University Journal of Agriculture and Nature* 24(6), 1333-1342. DOI: 10.18016/ksutarimdoga.vi.845203

Jobson, D. J., Rahman, Z. U., and Woodell, G. A. (1997a). "A multiscale retinex for bridging the gap between color images and the human observation of scenes," *IEEE Transactions on Image Processing* 6(7), 965-976. DOI: 10.1109/83.597272

Jobson, D. J., Rahman, Z. U., and Woodell, G. A. (1997b). "Properties and performance of a center/surround retinex," *IEEE Transactions on Image Processing* 6(3), 451-462. DOI: 10.1109/83.557356

Kaçamer, S., and Budakçı, M. (2023). "Application parameters of water transfer printing on wood-based panel surfaces," *BioResources* 18(1), 1025-1040. DOI: 10.15376/biores.18.1.1025-1040

Karamustafa, E. Y., Arsan, B., and Beşoğul, K. (2022). "The Impact of circular economy and Industry 4.0 on achievement of sustainable development goals: A systematic literature review," *Journal of Social Sciences* 24(2), 294-323. DOI: 10.54838/bilgisosyal.1113937

Katırcıoğlu, F. (2021). "Comparative analysis of retinex algorithms used in low-light color image enhancement," *Journal of Engineering Sciences and Research* 3(2), 188-206. DOI: 10.46387/bjesr.955356

Kok, M., and Young, T. M. (2014). "Evaluation of insect residue resistant coatings–Correlation of a screening method with a conventional assessment technique," *Progress in Organic Coatings* 77(9), 1382-1390. DOI: 10.1016/j.porgcoat.2014.04.020

Kurniawan, A., and Lubis, D. S. (2022). "Perancangan Corporate Identity Sebagai Media Promosi Pada UMKM Fajar Mebel Berbasis Adobe Photoshop Adobe Premiere Pro Dan Coreldraw," *CIVITAS: Jurnal Studi Manajemen* 4(1).

Land, E. H., and McCann, J. J. (1971). "Lightness and retinex theory," *J. Opt. Soc. Am.* 61(1), 1-11.

Li, M., Liu, J., Yang, W., Sun, X., and Guo, Z. (2018). "Structure-revealing low-light image enhancement via robust retinex model," *IEEE Transactions on Image Processing* 27(6), 2828-2841. DOI: 10.1109/TIP.2018.2810539

Ma, Q., Wang, Y., and Zeng, T. (2022). "Retinex-based variational framework for low-light image enhancement and denoising," *IEEE Transactions on Multimedia.* DOI: 10.1109/TMM.2022.3194993

Marco, J. M., Bellido-González, V., Sorzabal, I., Alonso, R., and Cueva, A. (2015). "Effects of ion bombardment pretreatment on glass coating processes and post tempering," DOI: 10.14332/svc15.proc.1935

Martinez, T., Bertron, A., Escadeillas, G., Ringot, E., and Simon, V. (2014). "BTEX abatement by photocatalytic TiO_2-bearing coatings applied to cement mortars," *Building and Environment* 71, 186-192. DOI: 10.1016/j.buildenv.2013.10.004

MathWorks (2023). "Image Processing Toolbox," (https://www.mathworks.com/products/image.html), accessed 01 Jan 2023.

Ng, Michael. K., and Wang, W. (2011). "A total variation model for Retinex," *SIAM Journal on Imaging Sciences* 4(1), 345-365. DOI: 10.1137/100806588

Rahman, Z. U., Jobson, D. J., and Woodell, G. A. (1996). "Multi-scale retinex for color image enhancement," *Proceedings of 3rd IEEE International Conference on Image Processing* 3, 1003-1006. DOI: 10.1109/ICIP.1996.560995

Redsve, I., Kuisma, R., Laitala, L., Pesonen-Leinonen, E., Mahlberg, R., Kymäläinen, H. R., and Sjöberg, A. M. (2003). "Application of a proposed standard for testing soiling and cleanability of resilient floor coverings," *Tenside, Surfactants, Detergents* 40(6), 346-352.

Rutherford, K. L., Trezona, R. I., Ramamurthy, A. C., and Hutchings, I. M. (1997). "The abrasive and erosive wear of polymeric paint films," *Wear* 203, 325-334. DOI: 10.1016/S0043-1648(96)07369-3

Santos, J. P., Paula, N. F., Pagani, R. A., Caldato, R. A., Da Silva, R., and Barrios, S. B. (2019). "Low-VOC coalescents," *Coating World-Technical Paper* 267-302.

Shi, H., Liu, F., and Han, E. H. (2011). "The corrosion behavior of zinc-rich paints on steel: Influence of simulated salts deposition in an offshore atmosphere at the steel/paint interface," *Surface and Coatings Technology* 205(19), 4532-4539. DOI: 10.1016/j.surfcoat.2011.03.118

TS EN 322 (1999). "Determination of moisture content of wood-based boards," Turkish Standards Institute, Ankara, Türkiye.

TS EN ISO 11998 (2006). "Paints and varnishes – Determination of wet-scrub resistance and cleanability of coatings," Turkish Standards Institute, Ankara, Türkiye.

Xu, J., Hou, Y., Ren, D., Liu, L., Zhu, F., Yu, M., and Shao, L. (2020a). "STAR: A structure and texture aware retinex model," *IEEE Transactions on Image Processing* 29, 5022-5037. DOI: 10.1109/TIP.2020.2974060

Xu, Y., Zhang, J., Ai, L., Lou, X., Lin, S., Lu, Y., and Song, W. (2020b). "Fabrication of mesoporous double-layer antireflection coatings with near-neutral color and application in crystalline silicon solar modules," *Solar Energy* 201, 149-156. DOI: 10.1016/j.solener.2020.02.098

Article submitted: July 17, 2023; Peer review completed: August 19, 2023; Revised version received and accepted: September 28, 2023; Published: December 15, 2023.
DOI: 10.15376/biores.19.1.1058-1078